

Impact of oxygen ordering on titanium lattice parameters

Martin S. Talla Noutack,¹ Fabienne Amann ,^{2,3} Sophie Nowak,⁴ Régis Poulain ,³ Raphaëlle Guillou,⁵ Stéphanie Delannoy,^{2,6} Ivan Guillot,³ Frédéric Prima,² and Emmanuel Clouet ^{1,*}

¹Université Paris-Saclay, CEA, Service de recherche en Corrosion et Comportement des Matériaux, SRMP, F-91191 Gif-sur-Yvette, France

²Université PSL, Chimie ParisTech, CNRS, IRCP (UMR 8247), F-75005 Paris, France

³Université Paris Est Creteil, CNRS, ICMPE (UMR 7182), 2 rue Henri Dunant, F-94320 Thiais, France

⁴Université Paris Cité, CNRS, ITODYS (UMR 7086), F-75013 Paris, France

⁵Université Paris-Saclay, CEA, Service de Recherche sur les Matériaux et procédés Avancés, F-91191 Gif-sur-Yvette, France

⁶Biotech Dental SAS, 305 allées de Craponne, F-13300 Salon-de-Provence, France



(Received 25 July 2023; accepted 8 January 2024; published 24 January 2024)

Variations with oxygen concentration of titanium lattice parameters are obtained by means of *ab initio* calculations, considering the impact of oxygen ordering. The quasiharmonic approximation is used to take into account the thermal expansion at finite temperature. Results show that lattice parameters depend mainly on oxygen concentration and, to a lesser extent, on the ordering state. Knowing these theoretical variations, one can get insights into the composition of ordered compounds existing in Ti-O binary alloys from their lattice mismatch measured experimentally by x-ray diffraction. The approach is used in a binary alloy containing 6000 ppm in weight of oxygen. It is concluded that the ordered compounds, which are observed after a recrystallization heat treatment, do not have the expected Ti₆O stoichiometry but have a composition close to the nominal concentration. Oxygen ordering proceeds, therefore, before oxygen partitioning in titanium.

DOI: [10.1103/PhysRevMaterials.8.013607](https://doi.org/10.1103/PhysRevMaterials.8.013607)

I. INTRODUCTION

Oxygen is one of the major hardening elements of titanium, used to strengthen the hcp α phase [1]. With a high solubility limit, more than 30 at.% at room temperature [2], titanium can incorporate a large amount of oxygen in its α matrix. But suboxide compounds with Ti₆O and Ti₃O stoichiometries are known to exist below the solubility limit [3–5]. These suboxides correspond to an ordering of the oxygen atoms which occupy the octahedral interstitial sites of the hcp lattice [6,7]. *Ab initio* calculations predict that these ordered compounds are the ground states in the titanium-rich part of the Ti-O phase diagram [8–10]. Although they have been known for a long time now, researchers rarely consider the existence of these ordered compounds when discussing the effect of oxygen on titanium properties, in particular the mechanical properties [11–16]. They generally assume that all oxygen is dissolved in a solid solution for the low concentrations encountered in titanium alloys, which are usually lower than 1 at.% (0.5 and 1 at.%, respectively, in grade-2 and -4 commercially pure Ti). But recent experiments have shown that ordered compounds can exist at room temperature in titanium for an oxygen concentration as low as 0.5 at.% [17], with potentially important consequences for titanium's mechanical properties [6,7,18,19]. These ordered compounds could be imaged by transmission electron microscopy through the superlattice reflections arising from oxygen ordering. Lattice mismatches between the ordered precipitates and the α matrix could also be measured at room temperature with x-ray

diffraction (XRD). But no information on their composition could be obtained. In particular, it remains unclear whether these ordered precipitates have a Ti₆O composition, as expected from thermodynamics [10], or whether their oxygen content is lower, with oxygen ordering proceeding before oxygen partitioning, i.e., with the formation of compounds having the same long-range order as Ti₆O ordered compounds but without reaching the Ti₆O stoichiometry. As oxygen addition is known to increase the lattice parameters of the Ti α phase, one can attempt to deduce the composition of ordered compounds from the lattice mismatches measured by XRD. But one first needs to better know the impact of oxygen ordering on titanium lattice parameters, in particular to be able to separate variations arising from oxygen ordering and from oxygen enrichment.

The aim of this article is to use *ab initio* calculations to fully relate the variations of titanium lattice parameters to oxygen concentration and order state. We first perform *ab initio* calculations at 0 K and then extend them at finite temperature, considering thermal expansion through the quasiharmonic approximation. The theoretical variations obtained for lattice parameters are finally compared to the ones measured by XRD in a Ti-O binary alloy at different temperatures, allowing us to make conclusions about the composition of the ordered compounds observed in this alloy.

II. PHASE STABILITY AND LATTICE PARAMETERS AT 0 K

A. DFT parameters

Ab initio calculations are performed within non-spin-polarized density functional theory (DFT) using the VASP

*Corresponding author: emmanuel.clouet@cea.fr

code [20]. The exchange and correlation functional is described with the generalized gradient approximation (GGA) as formulated by Perdew, Burke, and Ernzerhof (PBE) [21]. Considering the local density approximation (LDA) instead of GGA leads to the same impact of oxygen on titanium's lattice parameters at 0 K (Appendix B). Interactions between core and valence electrons are accounted for by the projector augmented wave method [22], with $3s$, $3p$, $3d$, and $4s$ orbitals treated as valence states for Ti and $2s$ and $2p$ treated as valence states for O. A plane wave cutoff energy equal to 500 eV is used for wave functions. A $24 \times 24 \times 18$ k -point grid generated with the Monkhorst-Pack [23] method is used for the primitive hcp Ti unit cell, and grids with similar k -point densities are used for supercells. Integration is performed with the Methfessel-Paxton broadening scheme, using a 0.1 eV width. According to our convergence tests, this leads to a precision better than 1 meV per atom for total energy differences. Each structure is fully relaxed, i.e., both periodicity vectors and atomic coordinates, to achieve a force convergence lower than 0.02 eV/\AA and an energy convergence of 10^{-6} eV. Although the supercells can theoretically become monoclinic during the relaxation, the underlying lattices remain always close to the initial hcp crystal, with only a small orthorhombicity, which may appear when the symmetry of the initial structure allows for different relaxations in different directions of the basal plane.

B. Phase stability

Oxygen occupies the octahedral interstitial sites of the hcp lattice formed by Ti atoms. The ground state with the lowest oxygen content is known to have Ti_6O stoichiometry [6–10]. It corresponds to a stacking along the $\langle c \rangle$ axis of basal layers with one third of their octahedral sites occupied by oxygen atoms alternating with oxygen free layers. Enriched basal layers are ordered with occupied octahedral sites separated by $\langle 1\bar{1}00 \rangle$ periodicity vectors [see the Ti_6O structure in Fig. 1(a)]. With A , B , and C denoting the three different octahedral sites in a basal layer, the Ti_6O ground state can be described by a periodic $AVBV$ stacking along the $\langle c \rangle$ axis, with A corresponding to a basal layer where A octahedral sites are occupied by O atoms and V meaning a layer where all octahedral sites are empty [Fig. 1(b)].

We check that our *ab initio* approach predicts the right ground state in the concentration range $0 \leq x_{\text{O}} \leq 1/6$, where $x_{\text{O}} = N_{\text{O}}/N_{\text{Ti}}$ is the occupation of the octahedral interstitial sites.¹ To this aim we calculate the formation energy of different ordered and disordered compounds. Disordered structures are built from a supercell corresponding to the $4 \times 4 \times 3$ repetition of the conventional hcp unit cell, with 96 Ti atoms. Oxygen atoms are placed on the octahedral sites with the special quasirandom structures (SQS) method [24] to obtain a random Ti-O solid solution. Ordered Ti_nO structures, with $n = 6, 12, 24, 48$, are built in the same supercell, starting from the Ti_6O ordered compound and depleting oxygen atoms regu-

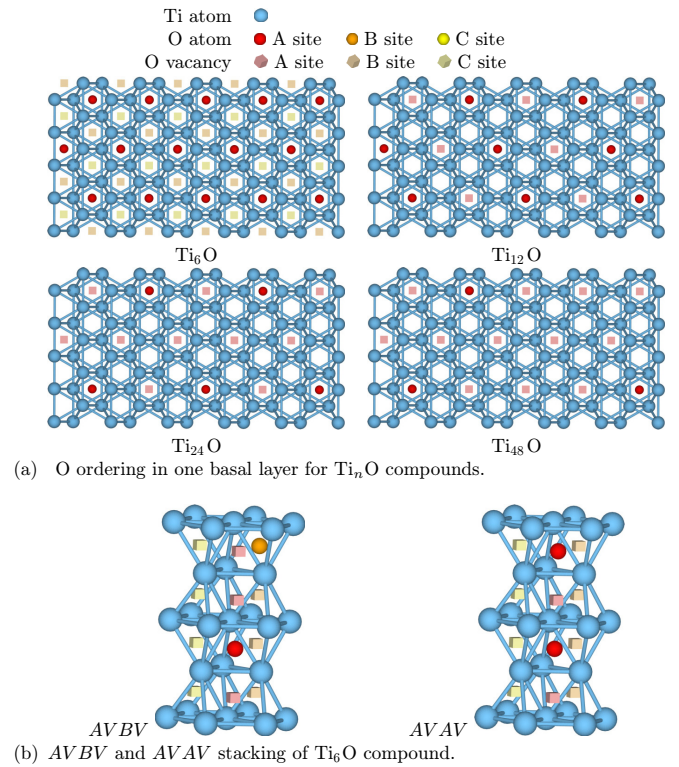


FIG. 1. Structures of ordered Ti_nO compounds. (a) Projection in the basal plane showing the periodic occupation by O atoms of octahedral interstitial sites for one basal layer. (b) $AVBV$ and (c) $AVAV$ stacking along the $\langle c \rangle$ axis of partially occupied basal layers. O atoms and empty octahedral sites are shown, respectively, with balls and cubes, using different colors for A , B , and C octahedral sites. B and C empty octahedral sites are shown only for the Ti_6O compound in (a).

larly in the basal layer, with either an $AVBV$ or $AVAV$ stacking along the $\langle c \rangle$ axis (Fig. 1). Finally, some partially ordered structures are also considered, using a larger supercell with 216 Ti atoms and incorporating some oxygen vacancies in the ordered Ti_6O compound.

Formation energies are calculated with reference to pure Ti and to the TiO compound, i.e., structures with all octahedral sites either empty ($x_{\text{O}} = 0$) or occupied by oxygen atoms ($x_{\text{O}} = 1$). Considering that the alloy is actually an oxygen-vacancy binary system on the octahedral interstitial sites of the hcp lattice formed by the Ti atoms, all formation energies are defined per interstitial site, leading to

$$E^f[\text{Ti}_n\text{O}_m] = \frac{1}{n} \left(E[\text{Ti}_n\text{O}_m] - \frac{n-m}{n} E[\text{Ti}_n] - \frac{m}{n} E[\text{Ti}_n\text{O}_n] \right),$$

where $E[\text{Ti}_n]$ and $E[\text{Ti}_n\text{O}_n]$ are the energies of pure Ti and TiO in the same supercell as the Ti_nO_m compound.

Figure 2 shows that ordered structures are always more stable than disordered solid solutions, confirming the ordering tendency of oxygen in titanium seen experimentally [4–6,17,25]. No intermediate compound is found below the convex hull linking Ti and Ti_6O , indicating that a supersaturated Ti(O) solid solution should decompose in an oxygen-depleted solution and an ordered Ti_6O compound at low temperature.

¹One can also define the oxygen concentration $c_{\text{O}} = N_{\text{O}}/(N_{\text{Ti}} + N_{\text{O}})$, i.e., the ratio of the number of oxygen atoms to the total number of atoms.

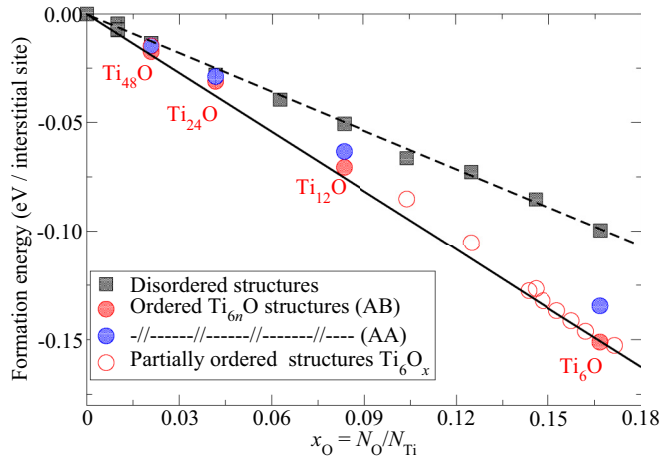


FIG. 2. Formation energies of different Ti_nO_m compounds as a function of oxygen occupation $x_O = m/n$ of interstitial sites. Symbols correspond to *ab initio* results for disordered, partly ordered, or completely ordered compounds. The solid black line indicates the convex hull linking most stable structures.

Considering now the different possible stackings along the $\langle c \rangle$ axis of oxygen-enriched basal layers, ordered compounds with an *AVBV* stacking are always more stable than *AVAV* stacking, in agreement with previous *ab initio* calculations [8–10] and with the stable structure known experimentally for Ti_6O . Nevertheless, the stacking of these basal layers offers more possibilities. *Ab initio* calculations for Ti_6O show that stackings in which two successive occupations of oxygen layers are different, i.e., *AVBV*, *AVBVCV*, and *AVBVCVBV*, lead to almost the same formation energy, with an energy difference lower than 1 meV/site, thus below the expected DFT accuracy (Table I). These ordered structures therefore appear to be degenerate, with *AVBV* stacking having the smallest wavelength along the $\langle c \rangle$ direction, leading to devil’s staircase [9] disordering at finite temperature.

C. Variations of lattice parameters

Ab initio calculations show that both a and c lattice parameters increase with the oxygen content (Fig. 3), with the parameter c increasing more rapidly than a , in agreement with experiments [2,26]. The comparison between experimental and theoretical values (Fig. 3) shows that *ab initio* calculations correctly predict the increase rates of both lattice parameters with the oxygen concentration, despite a slight underestimation of the absolute value. Because *ab initio* calculations are performed at 0 K, while experimental data were obtained at

TABLE I. Energy variation ΔE of the Ti_6O structures for different stackings of the oxygen-enriched basal layers along the $\langle c \rangle$ direction.

Stacking	ΔE (meV/site)
<i>AVBV</i>	0.
<i>AVAV</i>	14.72
<i>AVBVCV</i>	−0.93
<i>AVBVCVBV</i>	−0.66

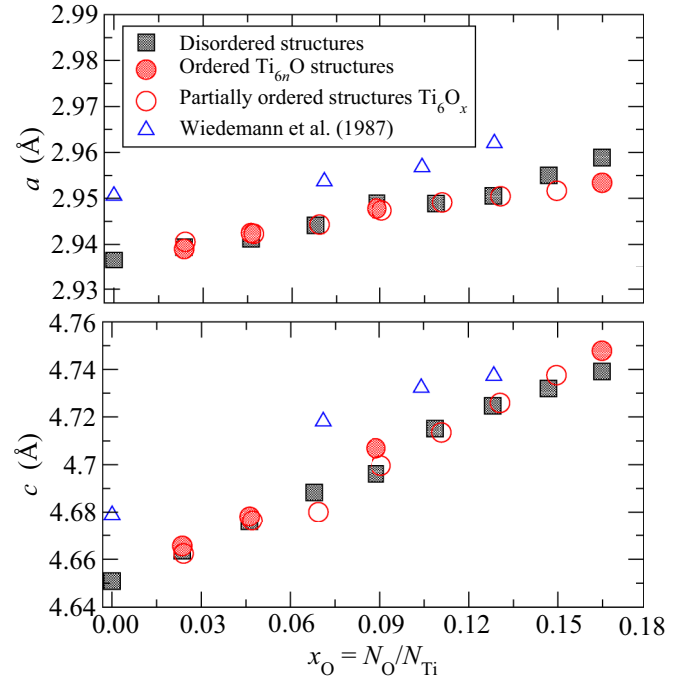


FIG. 3. Lattice parameters determined at 0 K by *ab initio* calculations for different compounds of the Ti-O binary alloy (squares and circles) compared to the experimental values determined at room temperature by Wiedemann *et al.* [26]. Similar experimental variations are shown in the review of Murray and Wriedt [2].

room temperature, such an underestimation is, indeed, expected. Besides, DFT approximation is known to be not fully quantitative when predicting absolute values for lattice parameters, with a dependence on the functional used for the electronic exchange and correlation (see Appendix B).

According to these *ab initio* calculations, the lattice parameters mainly depend on the oxygen concentration, with a marginal impact of the ordering state: for the same oxygen composition, a random solid solution and an ordered compound have almost the same lattice parameters at 0 K (Fig. 3). The only noticeable impact is on the highest oxygen concentrations, in particular for Ti_6O , where larger c and smaller a parameters are obtained for ordered compounds than for disordered solid solutions.

III. MODELING AT FINITE TEMPERATURES

A. Methods

To go beyond 0 K calculations, we now take into account thermal expansion by including the contribution of atomic vibrations in the formation free energy of the different compounds. Calculations are performed in the quasiharmonic approximation, as described below, considering different structures in the same supercell containing 72 Ti atoms and defined by the periodicity vectors $[\bar{2}200]$, $[0\bar{2}20]$, and $[\bar{1}103]$.

This is done by coupling PHONOPY [27] with VASP DFT calculations to obtain phonons for different volumes V and ratios $\gamma = c/a$ of the supercell. A finite displacement of 0.01 Å is used in PHONOPY to calculate the supercell force constants. Dynamical matrices $D(\vec{q})$ are then calculated by

TABLE II. Contributions to the free energy of electronic excitations F^{el} and of atomic vibrations F^{vib} calculated at different temperatures in pure Ti and in the ordered Ti_6O compound. Calculations are performed at the equilibrium volume and with the c/a ratio of the cohesive energy E^{coh} at 0 K.

T (K)	Free energies (meV/site)			
	Pure Ti		Ti_6O	
	F^{el}	F^{vib}	F^{el}	F^{vib}
0	0.0	0.7	0.0	46.8
300	-0.9	-45.7	-1.5	5.9
600	-4.1	-169.2	-3.8	-115.8
900	-10.0	-332.1	-8.7	-283.0

Fourier transformation on a regular \vec{q} grid with N_q points and diagonalized to obtain the pulsations $\omega_{\vec{q},s}$ of the eigenmodes. The vibration energy, defined per interstitial octahedral site, of a supercell containing n Ti atoms and m O atoms is finally given by

$$F^{\text{vib}}(V, \gamma, T) = \frac{1}{n} \frac{1}{N_{\vec{q}}} \sum_{\vec{q},s} \left\{ \frac{\hbar \omega_{\vec{q},s}(V, \gamma)}{2} + kT \ln \left[1 - \exp \left(-\frac{\hbar \omega_{\vec{q},s}(V, \gamma)}{kT} \right) \right] \right\}. \quad (1)$$

A $15 \times 15 \times 15$ \vec{q} grid is used for Fourier transform. Comparison with results obtained with $10 \times 10 \times 10$ and $20 \times 20 \times 20$ grids shows that this is enough for the supercell considered in this work.

The total free energy $F(V, \gamma, T) = E^{\text{coh}}(V, \gamma) + F^{\text{vib}}(V, \gamma, T)$ is obtained by adding the cohesive energy $E^{\text{coh}}(V, \gamma)$ directly given by DFT calculations. One could also consider the contribution F^{el} of electronic excitations to this free energy [28–30], but calculations performed for pure Ti and for the ordered Ti_6O compound show that this contribution can be neglected compared to the cohesive and vibrational contributions (Table II). The same conclusion was reached by Argaman *et al.* for pure Ti [31].

For each structure, the phonon spectrum is calculated on a 4×4 grid corresponding to four different volumes V and four different $\gamma = c/a$ ratios with a variation $\sim \pm 10\%$ around the equilibrium values of the cohesive energy. The free energy can then be defined on this (V, γ) grid for each temperature, and a continuous representation can be obtained thanks to a smooth interpolation with second-rank polynomials (Fig. 4). Minimization of this free energy finally leads to the equilibrium lattice parameters $a(T)$ and $c(T)$. As shown in Appendix A, this approach predicts lattice expansion in pure Ti, in agreement with experimental data (Fig. 10).

B. Variations of lattice parameters

Variations of lattice parameters with temperature are calculated for two different oxygen compositions, Ti_6O and Ti_{12}O , in addition to pure Ti. For each composition, we considered a random solid solution, as given by the SQS method, and a fully ordered structure with the most stable $AVBV$ stacking of the basal planes (Fig. 1). At 0 K, in the absence of atomic

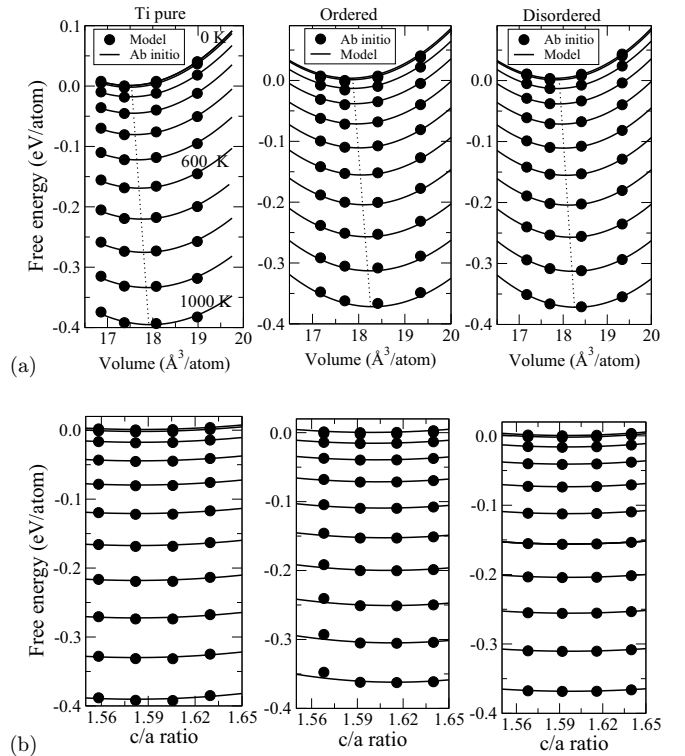


FIG. 4. Variation of the free energy with (a) the volume and (b) the $\gamma = c/a$ ratio for pure Ti (left), the ordered Ti_6O compound (center), and a disordered solid solution of composition Ti_6O (right). Free energies are shown every 100 K. Symbols are the direct results of *ab initio* calculations with quasiharmonic approximation, and lines show their interpolation. The c/a ratio and volume have been fixed to their 0 K equilibrium values in (a) and (b), respectively. The dashed line in (a) shows the position of the equilibrium volume for each temperature.

vibrations, the same variations of the lattice parameters with O concentration and ordering state (open symbols in Fig. 5) are observed as in the previous section (Fig. 3), thus showing that the obtained lattice parameters do not depend on the supercell used to model the different structures. Accounting for atomic vibrations does not modify how these lattice parameters vary qualitatively. The results confirm that lattice parameters increase with the oxygen content at all temperatures (Fig. 5), with variations which can be considered linear in both the disordered and ordered states. The impact of oxygen ordering is the same as the tendency observed at 0 K for the highest concentrations: the ordered state has a larger c and lower a lattice parameter than the disordered solid solution at the same oxygen concentration. This impact of oxygen ordering slightly increases with the temperature, as can be seen from the values of the slopes $\alpha_a^{\text{O}} = 1/a \partial a / \partial x_{\text{O}}$ and $\alpha_c^{\text{O}} = 1/c \partial c / \partial x_{\text{O}}$ given in Table III. The difference between the values for the ordered and disordered states increases with the temperature for both α_a^{O} and α_c^{O} . But this variation remains small and can be considered second order compared to the variation with the oxygen concentration.

To a good approximation, one can neglect the variations with the temperature of the increase rates α_a^{O} and α_c^{O} . The variations of the lattice parameters with the temperature and with

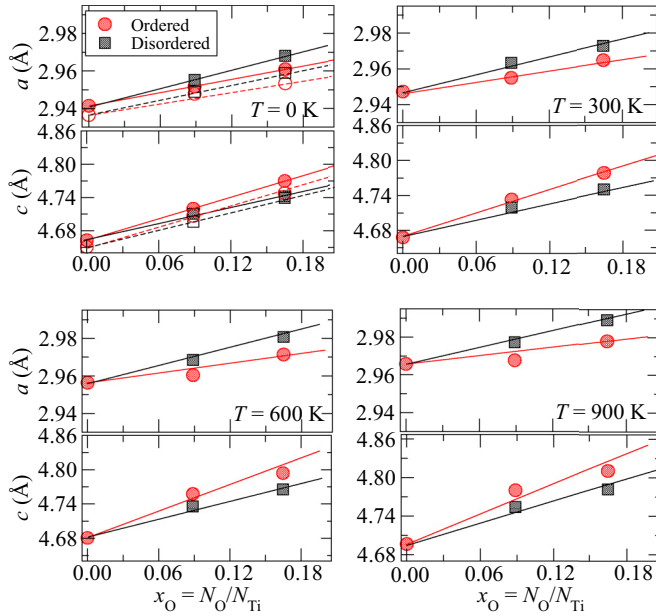


FIG. 5. Lattice expansion in Ti-O alloys as a function of oxygen content x_O . Red disks correspond to ordered compounds, and black squares correspond to disordered solid solutions, both calculated for the compositions Ti_{12}O and Ti_6O . Results in the absence of atomic vibrations, without zero-point energy, are indicated at 0 K by open symbols and dashed lines. Solid and dashed lines are linear fits of the corresponding data, imposing the lattice parameter of pure titanium in $x_O = 0$.

the oxygen concentration are then reasonably well described by the equations

$$a(T, x_O) = a_{\text{Ti}}^0 (1 + \alpha_a^T T) (1 + \alpha_a^O x_O), \quad (2)$$

$$c(T, x_O) = c_{\text{Ti}}^0 (1 + \alpha_c^T T) (1 + \alpha_c^O x_O), \quad (3)$$

showing that the increases with temperature T and with oxygen concentration x_O can be factorized. Parameters given in Table IV obtained through a fit of *ab initio* calculations confirm that a and c lattice parameters increase with the oxygen content, with a slightly higher (lower) increase rate of the c (a) parameter for the ordered states than for the disordered states.

IV. EXPERIMENTS AND DISCUSSION

A. Material and methods

XRD measurements are performed on titanium and a Ti-O binary alloy. The titanium, hereafter denoted pure titanium,

TABLE III. Slopes characterizing linear variations of lattice parameters a and c with O concentration, $\alpha_a^O = 1/a_{\text{Ti}} \partial a / \partial x_O$ and $\alpha_c^O = 1/c_{\text{Ti}} \partial c / \partial x_O$, shown in Fig. 5 for different temperatures.

TiO _x state		0 K	300 K	600 K	900 K
α_a^O	ordered TiO _x	0.040	0.035	0.028	0.022
	disordered TiO _x	0.055	0.055	0.049	0.048
α_c^O	ordered TiO _x	0.139	0.147	0.155	0.159
	disordered TiO _x	0.106	0.111	0.115	0.116

TABLE IV. Parameters entering Eq. (3) and describing the variations of Ti lattice parameters with temperature and oxygen content for the ordered and disordered states.

Phase	a parameter	c parameter
Pure Ti	$a_{\text{Ti}}^0 = 2.940 \text{ \AA}$ $\alpha_a^T = 9.4 \times 10^{-6} \text{ K}^{-1}$	$c_{\text{Ti}}^0 = 4.660 \text{ \AA}$ $\alpha_c^T = 8.3 \times 10^{-6} \text{ K}^{-1}$
Ordered TiO _x	$\alpha_a^O = 0.031$	$\alpha_c^O = 0.150$
Disordered TiO _x	$\alpha_a^O = 0.052$	$\alpha_c^O = 0.112$

contains only 600 wppm (weight ppm) oxygen, corresponding to an atomic composition $c_O = N_O / (N_{\text{Ti}} + N_O) = 0.18 \text{ at.}\%$ and to an occupation of interstitial octahedral sites $x_O = N_O / N_{\text{Ti}} = 0.18\%$, while the oxygen nominal concentration in the Ti-O alloy is 6000 wppm ($c_O = 1.77 \text{ at.}\%$ and $x_O = 1.81\%$). These concentrations are confirmed by inert gas fusion analysis. Both pure Ti and the Ti-O alloy are first hot- and cold-rolled with a thickness reduction of 75% and 40%, respectively, until we obtain 1 mm thick plates. The samples are then recrystallized in molten salt baths (Li_2CO_3 , Na_2CO_3 , K_2CO_3) at 1023 K for 600 s. After water quenching, both pure titanium and Ti-O samples present fully recrystallized α grains that are 90 and 30 μm in size, respectively. The samples are then polished with SiC grinding paper before a final polishing with a colloidal silica suspension.

XRD patterns are obtained with an XPert Pro Panalytical instrument operating at 40 kV and 40 mA. A cobalt source ($K\alpha_1 = 1.789 \text{ \AA}$ and $K\alpha_2 = 1.793 \text{ \AA}$) is used. The first diffractogram is recorded at room temperature without the heating chamber, so that the sample height can be adjusted after the installation of the chamber by comparing the peak positions. After the measurement at room temperature, an Anton Paar HTK 1200N furnace with a resistive system is used to heat the sample holder up to 473 K and then to different temperatures between 473 and 773 K at 10 K/min. The temperature measured on the sample holder could slightly differ from the sample temperature. The heating chamber is kept under argon flow to prevent oxidation. After 1 h of heating stabilization for each temperature, diffractograms are recorded in the $40^\circ - 90^\circ$ 2θ range with a 0.016° step size for 80 s. Five scans are recorded at each temperature step and then summed up for the analysis.

The lattice parameters of both the α matrix and ordered precipitates are determined thanks to a Rietveld refinement using the MAUD software. The refinement takes into account the nonmonochromatic feature of the x-ray beam and allows us to assign the shoulder to the right of the peaks to the $K\alpha_2$ ray of the cobalt source. The Caglioti parameters of the diffractometer are first calibrated with a LaB_6 powder. Crystallographic Open Database (COD) ID 9008517 is chosen for the crystal structure of the α matrix. Ordered precipitates have a Ti_6O structure, which corresponds to an ordering of the oxygen atoms in the octahedral interstitial sites of the hcp Ti -lattice [17]. The XRD pattern of the precipitate phase should theoretically display the same principal peaks as the α matrix, with some additional peaks arising from oxygen ordering. However, a previous study on the same Ti-O samples [17] showed that these additional peaks cannot be detected

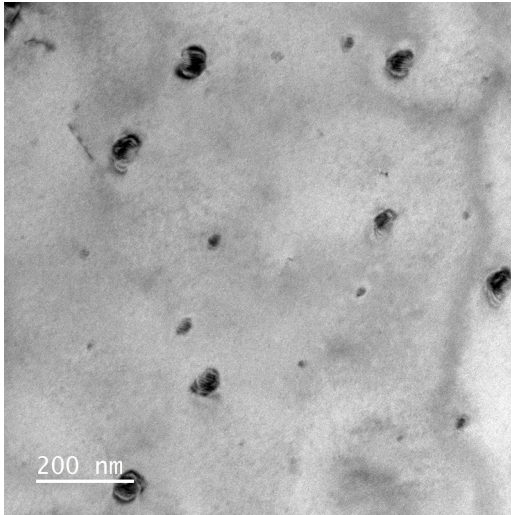


FIG. 6. TEM observation in the bright field mode of the Ti-O alloy.

by XRD because their intensity is too low and that Ti_6O -type precipitates can be characterized only by shoulders to the left of the matrix peaks, corresponding to slightly larger a and c lattice parameters of the underlying hcp lattice. Therefore, the same COD ID is used in the Rietveld refinement for the ordered precipitates as for the α matrix. Finally, the sample holder in alumina leads to some additional peaks which are taken into account in the Rietveld refinement by considering an Al_2O_3 phase (COD ID 1000059).

Transmission electron microscopy (TEM) observations of the Ti-O alloys are performed with a JEOL TEM after the recrystallization heat treatment using the same sample preparation as in Refs. [17,19].

B. Results

TEM observations confirm the presence of precipitates with a nanometric size (Fig. 6). These precipitates, which were previously imaged in dark field conditions using the superlattice diffraction of the Ti_6O ordered structure [17,32], can also be imaged in the bright field mode, thanks to their elastic strain field. This strain field arises from the lattice misfit between the ordered precipitates and the surrounding titanium matrix.

This lattice misfit leads to the presence of shoulder on the diffraction peaks in the XRD diffractograms (Fig. 7; see also Fig. 12 in Appendix C). This shoulder can clearly be seen to the left of the diffraction peak corresponding to the basal $\{0002\}$ planes ($44^\circ < 2\theta < 45^\circ$). It is the signature of the larger c lattice parameter of the ordered compounds compared to the one of the matrix. Note that this shoulder appearing for the basal $\{0002\}$ planes cannot be explained by a martensitic transformation of the hexagonal α phase to the orthorhombic α'' phase as such a transformation will lead to a splitting of all diffraction peaks except the ones corresponding to basal planes. This shoulder on $\{0002\}$ diffraction peaks can be explained only by a mixture of two phases with different c lattice parameters. Such a left shoulder is also visible on the peak corresponding to pyramidal $\{10\bar{1}1\}$ planes ($46.5^\circ < 2\theta < 47^\circ$).

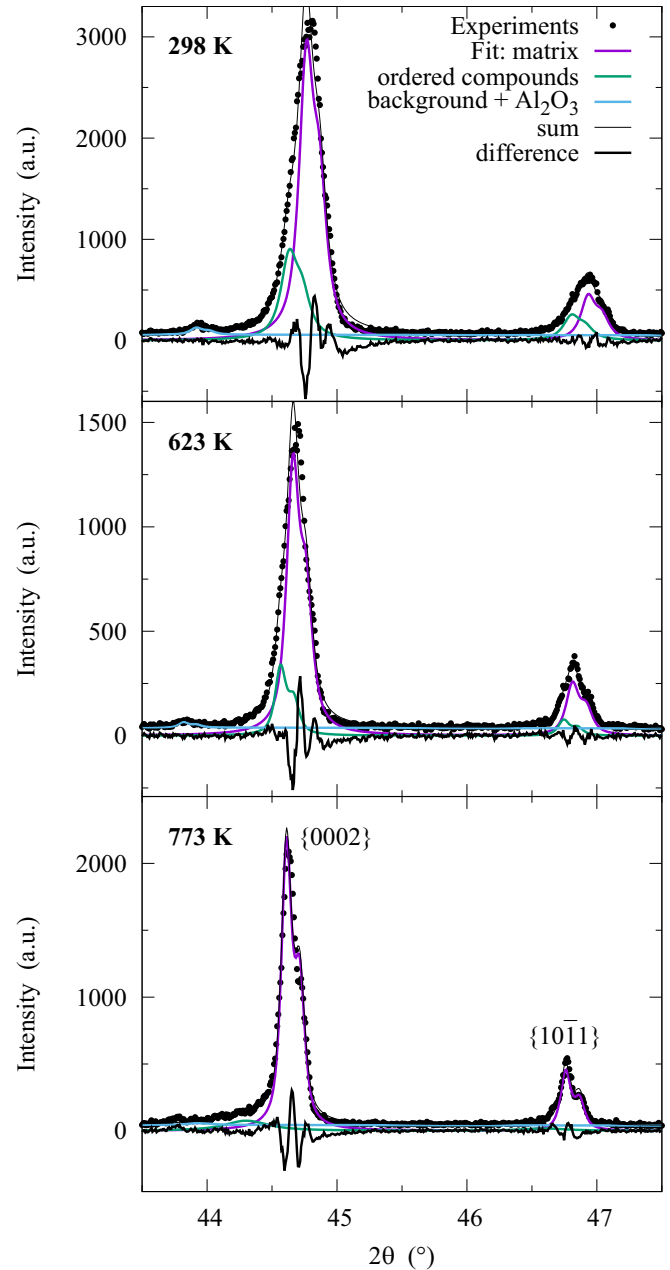


FIG. 7. X-ray diffraction patterns obtained at three different temperatures and their Rietveld refinements, showing the different contributions of the α -Ti matrix, the ordered compounds, and the alumina sample holder. These refinements lead to goodness of fit values [33] between 1.1 and 1.5.

On the other hand, because of the sample texture, the intensity of the peaks corresponding to $\{10\bar{1}0\}$ prismatic planes is not high enough to detect any shoulder. It is also observed that the signature of the ordered compounds is not very intense and almost disappears at 723 K and above (Fig. 12 in Appendix C), making analysis at these temperatures difficult. This is an indication that the ordered compounds have started to dissolve and that the O solubility limit at these temperatures is higher than the sample nominal concentration, i.e., 6000 wppm, which looks reasonable according to the theoretical phase diagram [10]. Such a dissolution of ordered precipitates was also seen

TABLE V. Experimental values of lattice parameters deduced from MAUD Rietveld refinement and oxygen content $x_O = N_O/N_{Ti}$ deduced from these measurements using Eq. (4).

T (K)	Sample	Phase	a (Å)			c (Å)			x_O
298	pure Ti	matrix	2.9536	±	1×10^{-4}	4.6850	±	1×10^{-4}	0.012
	Ti-O	matrix	2.9501	±	1×10^{-4}	4.6929	±	1×10^{-4}	
	Ti-O	compounds	2.9575	±	2×10^{-4}	4.7061	±	2×10^{-4}	
473	pure Ti	matrix	2.9586	±	1×10^{-4}	4.6913	±	1×10^{-4}	0.013
	Ti-O	matrix	2.9551	±	1×10^{-4}	4.6999	±	1×10^{-4}	
	Ti-O	compounds	2.9566	±	3×10^{-4}	4.7125	±	2×10^{-4}	
523	pure Ti	matrix	2.9596	±	1×10^{-4}	4.6937	±	1×10^{-4}	0.013
	Ti-O	matrix	2.9567	±	1×10^{-4}	4.7022	±	1×10^{-4}	
	Ti-O	compounds	2.9642	±	6×10^{-4}	4.7146	±	2×10^{-4}	
573	pure Ti	matrix	2.9610	±	1×10^{-4}	4.6960	±	1×10^{-4}	0.013
	Ti-O	matrix	2.9577	±	1×10^{-4}	4.7045	±	1×10^{-4}	
	Ti-O	compounds	2.9651	±	7×10^{-4}	4.7132	±	2×10^{-4}	
598	pure Ti	matrix	2.9613	±	1×10^{-4}	4.6966	±	1×10^{-4}	0.015
	Ti-O	matrix	2.9594	±	1×10^{-4}	4.7060	±	1×10^{-4}	
	Ti-O	compounds	2.9624	±	4×10^{-4}	4.7156	±	2×10^{-4}	
623	pure Ti	matrix	2.9616	±	1×10^{-4}	4.6977	±	1×10^{-4}	0.016
	Ti-O	matrix	2.9600	±	1×10^{-4}	4.7075	±	1×10^{-4}	
	Ti-O	compounds	2.9634	±	3×10^{-4}	4.7170	±	2×10^{-4}	
648	pure Ti	matrix	2.9621	±	1×10^{-4}	4.6986	±	1×10^{-4}	0.017
	Ti-O	matrix	2.9608	±	1×10^{-4}	4.7087	±	1×10^{-4}	
	Ti-O	compounds	2.9645	±	3×10^{-4}	4.7169	±	2×10^{-4}	
673	pure Ti	matrix	2.9626	±	1×10^{-4}	4.6993	±	1×10^{-4}	0.015
	Ti-O	matrix	2.9607	±	1×10^{-4}	4.7086	±	1×10^{-4}	
	Ti-O	compounds	2.9640	±	3×10^{-4}	4.7170	±	2×10^{-4}	
698	pure Ti	matrix	2.9630	±	1×10^{-4}	4.7002	±	1×10^{-4}	0.019
	Ti-O	matrix	2.9623	±	1×10^{-4}	4.7115	±	1×10^{-4}	
	Ti-O	compounds	2.9671	±	5×10^{-4}	4.7186	±	4×10^{-4}	
723	pure Ti	matrix	2.9636	±	1×10^{-4}	4.7014	±	1×10^{-4}	0.019
	Ti-O	matrix	2.9625	±	1×10^{-4}	4.7128	±	1×10^{-4}	
	Ti-O	compounds	2.9642	±	1×10^{-4}	4.7224	±	4×10^{-4}	
748	pure Ti	matrix	2.9642	±	1×10^{-4}	4.7025	±	1×10^{-4}	0.010
	Ti-O	matrix	2.9632	±	1×10^{-4}	4.7083	±	1×10^{-4}	
	Ti-O	compounds	2.9643	±	1×10^{-4}	4.7451	±	7×10^{-4}	
773	pure Ti	matrix	2.9646	±	1×10^{-4}	4.7036	±	1×10^{-4}	0.020
	Ti-O	matrix	2.9646	±	1×10^{-4}	4.7150	±	1×10^{-4}	
	Ti-O	compounds	2.9739	±	4×10^{-4}	4.7493	±	6×10^{-4}	

recently in a Ti-Zr-O alloy using TEM and resistivity with *in situ* heating experiments [34].

Rietveld refinement of XRD diffractograms allows extracting the lattice parameters a and c of pure Ti, as well as of both the matrix and the ordered compounds in the Ti-O alloy (Table V). As expected, the ordered compounds have larger lattice parameters than the matrix in the Ti-O alloy for all the considered temperatures. To compare the lattice parameters measured in the Ti-O alloy with the ones deduced from *ab initio* calculations, we compute the differences δa and δc between the parameters measured in the alloy and in pure Ti at the same temperature, as these variations are less sensitive to the choice of the exchange-correlation functional used for *ab initio* calculations than absolute values of a and c (see Appendix B). We neglect, for the experimental data, the presence of 0.18 at.% oxygen in pure Ti, as it has only a marginal impact on the obtained δa and δc values. δa and δc characterize the increase in lattice parameters induced by

the presence of oxygen. The increase δc measured for the matrix phase is almost constant with temperature, and its value corresponds to the theoretical one obtained for a random solid solution with the same nominal concentration as the Ti-O alloy (Fig. 8). This is a strong indication that there is no real oxygen depletion in the matrix despite the presence of ordered compounds. The experimental lattice increases δc obtained for the compounds are higher than the ones for the matrix but do not reach the theoretical values expected for ordered compounds with a Ti_6O stoichiometry (Fig. 8). Although these compounds are enriched in oxygen, they do not have the expected 1/6 stoichiometry. The same conclusions can be drawn from the obtained δa lattice increase, although things are less clear. The uncertainty comes from the smallest expected values for δa compared with those of δc because the impact of oxygen is smaller on a than on c , as already shown before (Fig. 5). Besides, because the sample texture leads to the absence of the prismatic peak, the experimental precision

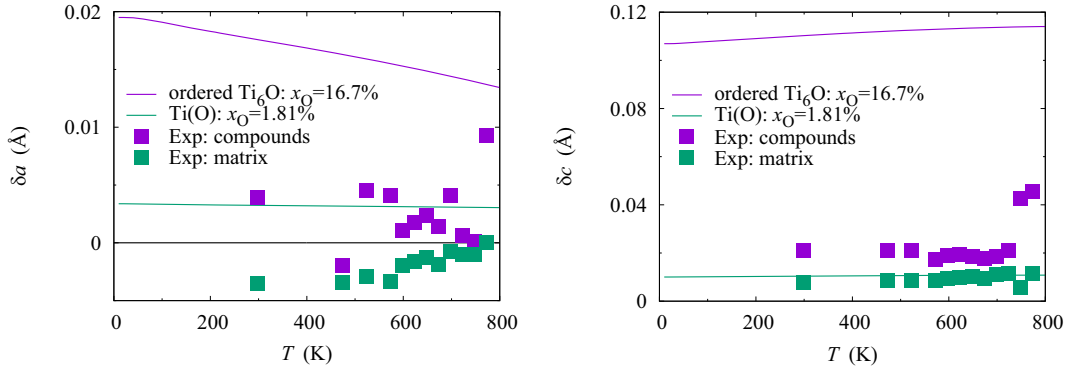


FIG. 8. Increase in lattice parameters a and c induced by oxygen as a function of the temperature. Lines are the predictions of the *ab initio* model for the ordered Ti_6O compound (purple line) and for a random solid solution of composition $x_{\text{O}} = 1.81\%$ (green line). Symbols are results of experiments for the ordered compounds and for the matrix.

on a is not as high as on c , explaining why slightly negative values are obtained for δa in the matrix when a lattice increase is expected.

C. Discussion

Despite the uncertainty existing in both the theoretical and experimental variations of Ti lattice parameters with the oxygen content and with the ordering state, one can try to determine the composition of the ordered compounds and of the matrix from the increases δa and δc in the lattice parameters, which were measured by XRD at the different temperatures. A least squares fit of both the a and c parameters leads to the following expression for the occupation of the octahedral interstitial sites:

$$x_{\text{O}}(\delta a, \delta c) = \frac{a_{\text{Ti}} \alpha_a^{\text{O}} \delta a + c_{\text{Ti}} \alpha_c^{\text{O}} \delta c}{(a_{\text{Ti}} \alpha_a^{\text{O}})^2 + (c_{\text{Ti}} \alpha_c^{\text{O}})^2}. \quad (4)$$

Using the lattice parameters of pure Ti, a_{Ti} and c_{Ti} , determined experimentally at each temperature with the theoretical lattice increases α_a^{O} and α_c^{O} given in Table IV, thus neglecting their variation with the temperature, one obtains the compositions x_{O} given in Table V and shown in Fig. 9. These results confirm that the ordered compounds have a lower composition than the expected value $x_{\text{O}} = 1/6 \sim 0.167$ corresponding to Ti_6O stoichiometry. Their composition starts to rise at the two highest temperatures considered in this study, 748 and 773 K, but without reaching the Ti_6O composition. However, as noted before, the intensity of the diffraction peaks assigned to the ordered compounds is not very intense at these two temperatures (Fig. 12 in Appendix C), and one cannot expect an accurate determination of the corresponding lattice parameters at these high temperatures where the ordered compounds have probably started to dissolve. Figure 9 also illustrates that this approach to determine the composition of the matrix and of the ordered compounds cannot be considered fully quantitative: at low temperature, one observes an oxygen depletion of the matrix and an enrichment of the compounds, as expected, but at the highest temperatures, both phases are enriched, which violates the conservation law. This uncertainty of the obtained composition arises from the difficulty of deconvoluting the x-ray diffraction pattern to associate

different lattice parameters with different phases; the closer the lattice parameters are, the more difficult it is. It is also hard to reach a precision high enough in the *ab initio* determination of the increase rates α_a^{O} and α_c^{O} , especially for such small variations of the lattice parameters. Finally, when deriving the composition from measured lattice parameters, we assume that the different phases are free of stress, which is not true for coherent compounds embedded in a matrix. Nevertheless, despite all the remaining uncertainties, the approach allows us to conclude that the ordered compounds do not have the Ti_6O composition and are only slightly enriched with oxygen compared to the surrounding matrix.

As shown in Ref. [17] with electronic diffraction, these ordered compounds, which can be found in binary Ti-O alloys, have a crystallographic structure corresponding to the one known for Ti_6O crystal (space group $P31c$). Although the binary phase diagram predicts that the equilibrium composition of these ordered compounds should be close to Ti_6O stoichiometry [10], the present work shows that these precipitates do not have this composition. One possibility is that oxygen diffusion is not fast enough to reach

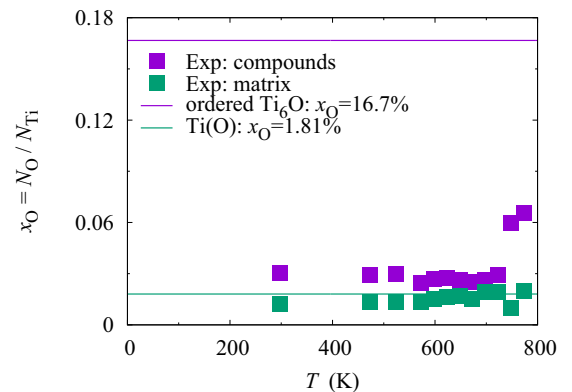


FIG. 9. Oxygen content x_{O} of the matrix and of the ordered compounds determined with Eq. (4) from the experimental lattice parameters (Table V) and from the theoretical increase rates α_a^{O} and α_c^{O} (Table IV). The horizontal lines correspond to the nominal composition $x_{\text{O}} = 0.0181$ of the Ti-O alloy and to the composition of stoichiometric Ti_6O compounds ($x_{\text{O}} = 1/6 \sim 0.167$).

thermal equilibrium. Considering the oxygen diffusion coefficient $D_O(T) = D_O^0 \exp(-Q_O/RT)$ with an activation energy $Q_O = 200 \text{ kJ mol}^{-1}$ and a diffusion preexponential constant $D_O^0 = 4.5 \times 10^{-5} \text{ m}^2 \text{ s}^{-1}$ [35], one can estimate the mean square displacement of oxygen atoms when diffusing a time lapse Δt , $d_O(T, \Delta t) = \sqrt{6D_O(T) \Delta t}$. For the recrystallization heat treatment ($T = 1023 \text{ K}$ and $\Delta t = 600 \text{ s}$), the oxygen mean square displacement is $3 \text{ }\mu\text{m}$, thus showing that equilibrium is reached. But according to the theoretical phase diagram [10], this temperature is too high for Ti_6O ordered compounds to be stable. The disappearance of the signature of this ordered phase in the diffraction patterns above 723 K is also a strong indication that Ti_6O compounds are not stable at the recrystallization temperature. The ordered compounds should instead appear during the quench, when the temperature becomes low enough to lead to the decomposition of the initial homogeneous solid solution in a depleted solid solution and an ordered phase with Ti_6O -type crystallographic structure. If the subsequent quench is fast enough, which should be true for the water quench used here, one does not expect the forming precipitates to reach equilibrium, thus explaining why the observed ordered compounds have a lower composition than the expected Ti_6O stoichiometry.

Considering now the holds ($\Delta t = 3600 \text{ s}$) at different temperatures for the XRD measurements, the composition of the precipitates remains almost unchanged up to 723 K (Fig. 9), with the signature of the ordered compounds in the XRD pattern disappearing at this temperature and above (Fig. 12 in Appendix C). Oxygen diffusion should be too slow below 723 K to allow for a change in precipitates. This appears reasonable as the oxygen mean square displacement is only 60 nm at $T = 723 \text{ K}$. At this temperature and above, it appears high enough to allow for precipitate evolution, in particular precipitate dissolution, but not below it. Better characterization of the kinetic evolution of the ordered compounds will require additional experimental techniques like synchrotron XRD with *in situ* heating to follow more precisely the evolution of the matrix and compounds lattice parameters, and hence of their composition, during the different heat treatments. *In situ* heating experiments in a TEM are also appealing to image the evolution of these precipitates, in particular their size, shape, and density. Once the thermal conditions have been found to get closer to equilibrium without dissolving the precipitates, it should be possible to use analytical TEM or atom probe tomography to check that equilibrium precipitates have a composition close to Ti_6O stoichiometry, as expected from the equilibrium phase diagram [10].

V. CONCLUSIONS

Ab initio calculations correctly predict an increase in the titanium lattice parameters with the oxygen concentration for compositions between pure Ti and Ti_6O . The increase is more important for c than for the a parameter, in agreement with experiments. The ordering state of oxygen atoms in the octahedral sites of the hcp lattice influences these lattice parameters, but the impact is less important than that of oxygen concentration: for the same oxygen composition, an ordered compound has a slightly larger (lower) c parameter (a pa-

rameter). This is true both at 0 K and at finite temperature, when lattice expansion is considered in the *ab initio* approach through the quasiharmonic approximation.

Knowing the impact of both oxygen concentration and oxygen ordering on lattice parameters, it is theoretically possible to relate the lattice mismatches of ordered compounds existing in Ti-O binary alloys to their composition. Although the approach cannot be fully quantitative because of the limited accuracy of *ab initio* phonon calculations and their difficulty predicting small variations in lattice parameters, it nevertheless leads to new information on the composition of the different phases. Applying the approach to an alloy containing 6000 wppm O ($x_O = 1.81\%$), one can conclude that the ordered compounds, which are present after a heat treatment at 1023 K followed by a water quench, do not have the expected Ti_6O stoichiometry, but a composition close to the alloy's nominal concentration. This makes these precipitates undetectable by experimental techniques which are sensitive only to chemistry, like analytical TEM or atom probe tomography. Oxygen ordering proceeds therefore at a faster pace than partitioning in this alloy: these precipitates have long-range order corresponding to the Ti_6O structure, as previously shown with TEM [17], but their composition is lower than the equilibrium one corresponding to Ti_6O stoichiometry. These precipitates, which are out of equilibrium and probably appear during the quench following the recrystallization heat treatment, do not evolve until reaching temperatures high enough to allow for significant diffusion of oxygen, i.e., above 723 K . It remains to be found in more detail how the thermomechanical processing, in particular the temperature and duration of the annealing or the cooling speed, impacts the composition of these ordered compounds.

ACKNOWLEDGMENTS

This work was performed using HPC resources from GENCI-IDRIS and -TGCC (Grant No. 2022-096847). The

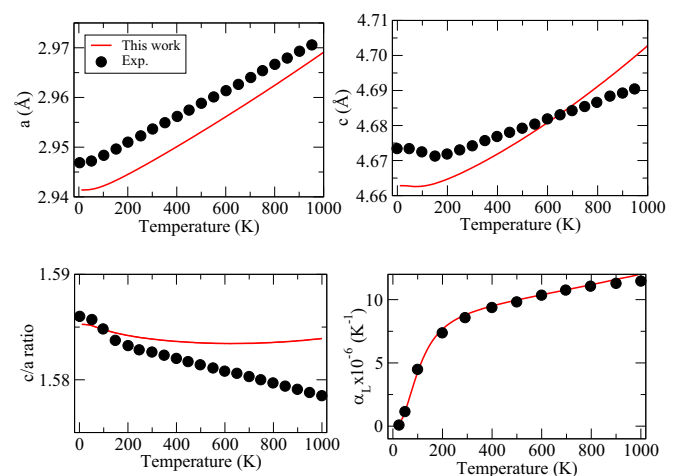


FIG. 10. Lattice expansion of pure titanium as predicted by *ab initio* calculations with the quasiharmonic approximation (lines) and compared to the experimental data using the recommended values of Touloukian *et al.* [36].

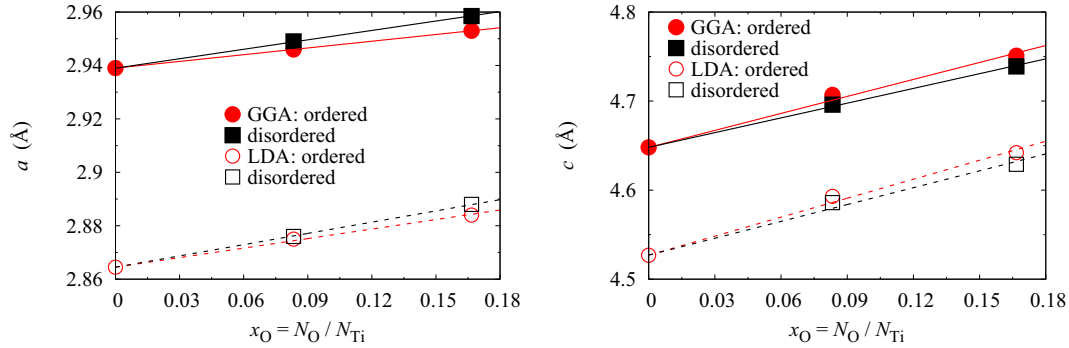


FIG. 11. Variations of a and c lattice parameters with O concentration for ordered and disordered structures calculated at 0 K with two different exchange-correlation functionals, GGA-PBE (solid symbols and solid lines) and LDA (open symbols and dashed lines). Lines are the fit of the *ab initio* calculations, imposing the lattice parameters of pure Ti for $x_O = 0$.

French National Research Agency (ANR) is acknowledged for the funding of the TiTol Project (Grant No. ANR-19-CE08-0032). Y. Millet from the Timet company is gratefully acknowledged for providing the alloys studied in this work.

APPENDIX A: LATTICE EXPANSION OF PURE Ti

We examine in this Appendix how quantitative our modeling approach relying on *ab initio* calculations and the quasiharmonic approximation to predict the variations with temperature of the lattice parameters is, considering pure Ti, for which experimental data can be found [36]. Calculations were performed in a supercell containing 96 Ti atoms, which is a $4 \times 4 \times 3$ replication of the conventional hcp unit cell. As shown in Fig. 10, the model reproduces the experimental data reasonably well, particularly the anisotropy of the linear expansion characterized by a decreasing c/a ratio with temperature and a contraction of the c parameter at very low temperature, in agreement with previous *ab initio* calculations [31,37,38]. The best agreement is found for the variations of the volume V with the temperature, as characterized by the average linear expansion

$$\alpha_L = \frac{1}{3V} \left. \frac{\partial V}{\partial T} \right|_P.$$

APPENDIX B: IMPACT OF THE EXCHANGE-CORRELATION FUNCTIONAL

Equilibrium lattice parameters obtained from *ab initio* calculations are known to depend on the functional used to describe the electronic exchange and correlation. To test how the exchange-correlation functional impacts the obtained variations of the lattice parameters, we have performed additional calculations using the LDA with the parametrization of Perdew and Zunger [39]. Except for the exchange-correlation functional, the *ab initio* parameters are the same as for GGA calculations. Calculations were performed at 0 K, neglecting atomic vibrations, for pure Ti, Ti_{12}O , and Ti_6O , considering a disordered state (SQS) and an ordered state. The structures, which rely on a 72 atom supercell, are the same as the ones described in Sec. III A. As expected, the LDA functional leads

to slightly smaller lattice parameters than GGA (Fig. 11). But looking now at relative variations, one sees that LDA and GGA lead to the same linear variations with the oxygen content. The lines describing these linear variations are parallel, with only an offset corresponding to the different lattice parameters predicted by LDA and GGA for pure Ti. This is true for both the ordered and disordered states, with the increase rate of the a (c) lattice parameter being slightly higher (lower) for the disordered state than for the ordered state. As long as one works with the lattice increases δa and

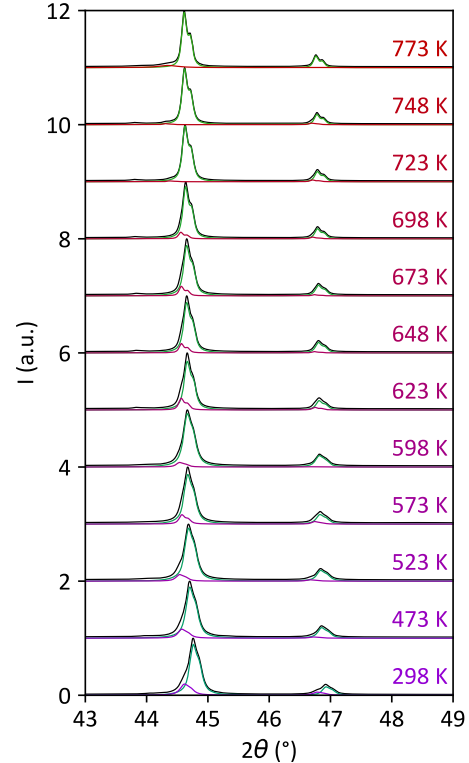


FIG. 12. X-ray diffraction patterns obtained at different temperatures in the Ti-O alloy. For each temperature, the experimental diffractogram (black) is shown with the contributions of the α -Ti matrix (green) and the ordered compounds (purple) obtained from Rietveld refinement.

δc induced by oxygen, there is no impact of the exchange-correlation functional used for *ab initio* calculations, at least when considering LDA and GGA-PBE functionals.

APPENDIX C: XRD DATA

Figure 12 shows x-ray diffraction patterns obtained at different temperatures in the Ti-O alloy.

- [1] H. Conrad, Effect of interstitial solutes on the strength and ductility of titanium, *Prog. Mater. Sci.* **26**, 123 (1981).
- [2] J. L. Murray and H. A. Wriedt, The O-Ti (oxygen-titanium) system, *J. Phase Equilib.* **8**, 148 (1987).
- [3] I. I. Kornilov and V. V. Glazova, Phase diagram of the system Ti-O₂ and some properties of the alloys of this system, in *Physical Metallurgy of Titanium*, edited by I. I. Kornilov (Izdatell'stvo Nauka, Moscow, 1965), pp. 12–28.
- [4] S. Yamaguchi, M. Koiwa, and M. Hirabayashi, Interstitial superlattice of Ti₆O and its transformation, *J. Phys. Soc. Jpn.* **21**, 2096 (1966).
- [5] S. Yamaguchi, Interstitial order-disorder transformation in the Ti-O solid solution. I. Ordered arrangement of oxygen, *J. Phys. Soc. Jpn.* **27**, 155 (1969).
- [6] M. Hirabayashi, S. Yamaguchi, H. Asano, and K. Hiraga, Order-disorder transformations of interstitial solutes in transition metals of IV and V groups, in *Order-Disorder Transformations in Alloys* (Springer, Berlin, 1974), pp. 266–302.
- [7] S. Banerjee and P. Mukhopadhyay, *Phase Transformations: Examples from Titanium and Zirconium Alloys*, edited by R. W. Cahn, Pergamon Materials Series Vol. 12 (Elsevier, Amsterdam, 2007).
- [8] A. V. Ruban, V. I. Baykov, B. Johansson, V. V. Dmitriev, and M. S. Blanter, Oxygen and nitrogen interstitial ordering in hcp Ti, Zr, and Hf: An *ab initio* study, *Phys. Rev. B* **82**, 134110 (2010).
- [9] B. P. Burton and A. van de Walle, First principles phase diagram calculations for the octahedral-interstitial system α TiO_x, $0 \leq x \leq 1/2$, *CALPHAD: Comput. Coupling Phase Diagrams Thermochem.* **39**, 97 (2012).
- [10] N. S. H. Gunda, B. Puchala, and A. Van der Ven, Resolving phase stability in the Ti-O binary with first-principles statistical mechanics methods, *Phys. Rev. Mater.* **2**, 033604 (2018).
- [11] Q. Yu, L. Qi, T. Tsuru, R. Traylor, D. Rugg, J. W. Morris, Jr., M. Asta, D. C. Chrzan, and A. M. Minor, Origin of dramatic oxygen solute strengthening effect in titanium, *Science* **347**, 635 (2015).
- [12] B. Barkia, V. Doquet, J.-P. Couzinié, I. Guillot, and E. Héripé, In situ monitoring of the deformation mechanisms in titanium with different oxygen contents, *Mater. Sci. Eng., A* **636**, 91 (2015).
- [13] B. Barkia, J.-P. Couzinié, S. Lartigue-Korinek, I. Guillot, and V. Doquet, In situ TEM observations of dislocation dynamics in α titanium: Effect of the oxygen content, *Mater. Sci. Eng., A* **703**, 331 (2017).
- [14] N. Chaari, D. Rodney, and E. Clouet, Oxygen-dislocation interaction in titanium from first principles, *Scr. Mater.* **162**, 200 (2019).
- [15] Y. Chong, M. Poschmann, R. Zhang, S. Zhao, M. S. Hooshmand, E. Rothchild, D. L. Olmsted, J. W. Morris, Jr., D. C. Chrzan, M. Asta, and A. M. Minor, Mechanistic basis of oxygen sensitivity in titanium, *Sci. Adv.* **6**, eabc4060 (2020).
- [16] Y. Chong, R. Gholizadeh, T. Tsuru, R. Zhang, K. Inoue, W. Gao, A. Godfrey, M. Mitsuhashi, J. W. Morris, Jr., A. M. Minor, and N. Tsuji, Grain refinement in titanium prevents low temperature oxygen embrittlement, *Nat. Commun.* **14**, 404 (2023).
- [17] R. Poulain, S. Delannoy, I. Guillot, F. Amann, R. Guillou, S. Lartigue-Korinek, D. Thiaudière, J.-L. Béchade, E. Clouet, and F. Prima, First experimental evidence of oxygen ordering in dilute titanium–oxygen alloys, *Mater. Res. Lett.* **10**, 481 (2022).
- [18] I. I. Kornilov, Effect of oxygen on titanium and its alloys, *Met. Sci. Heat Treat.* **15**, 826 (1973).
- [19] F. Amann, R. Poulain, S. Delannoy, J.-P. Couzinié, E. Clouet, I. Guillot, and F. Prima, An improved combination of tensile strength and ductility in titanium alloys via oxygen ordering, *Mater. Sci. Eng. A* **867**, 144720 (2023).
- [20] G. Kresse and J. Furthmüller, Efficiency of *ab-initio* total energy calculations for metals and semiconductors using a plane-wave basis set, *Comput. Mater. Sci.* **6**, 15 (1996).
- [21] J. P. Perdew, K. Burke, and M. Ernzerhof, Generalized gradient approximation made simple, *Phys. Rev. Lett.* **77**, 3865 (1996).
- [22] P. E. Blöchl, Projector augmented-wave method, *Phys. Rev. B* **50**, 17953 (1994).
- [23] H. J. Monkhorst and J. D. Pack, Special points for Brillouin-zone integrations, *Phys. Rev. B* **13**, 5188 (1976).
- [24] A. van de Walle, P. Tiwary, M. de Jong, D. L. Olmsted, M. Asta, A. Dick, D. Shin, Y. Wang, L.-Q. Chen, and Z.-K. Liu, Efficient stochastic generation of special quasirandom structures, *CALPHAD: Comput. Coupling Phase Diagrams Thermochem.* **42**, 13 (2013).
- [25] S. Yamaguchi, K. Hiraga, and M. Hirabayashi, Interstitial order-disorder transformation in the Ti-O solid solution. IV. A neutron diffraction study, *J. Phys. Soc. Jpn.* **28**, 1014 (1970).
- [26] K. E. Wiedemann, R. N. Shenoy, and J. Unnam, Microhardness and lattice parameter calibrations of the oxygen solid solutions of unalloyed α -titanium and Ti-6Al-2Sn-4Zr-2Mo, *Metall. Trans. A* **18**, 1503 (1987).
- [27] A. Togo and I. Tanaka, First principles phonon calculations in materials science, *Scr. Mater.* **108**, 1 (2015).
- [28] C. Wolverton and A. Zunger, First-principles theory of short-range order, electronic excitations, and spin polarization in Ni-V and Pd-V alloys, *Phys. Rev. B* **52**, 8813 (1995).
- [29] X. Zhang, B. Grabowski, F. Körmann, C. Freysoldt, and J. Neugebauer, Accurate electronic free energies of the *3d*, *4d*, and *5d* transition metals at high temperatures, *Phys. Rev. B* **95**, 165126 (2017).
- [30] M. Cottura and E. Clouet, Solubility in Zr-Nb alloys from first-principles, *Acta Mater.* **144**, 21 (2018).
- [31] U. Argaman, E. Eidelstein, O. Levy, and G. Makov, *Ab initio* study of the phononic origin of negative thermal expansion, *Phys. Rev. B* **94**, 174305 (2016).
- [32] R. Poulain, Conception et développement d'une nouvelle famille d'alliages de titane à haute résistance mécanique et biocompatibilité optimisée pour l'implantologie dentaire, Ph.D. thesis, Université PSL, 2020.

- [33] B. H. Toby, *R* factors in Rietveld analysis: How good is good enough? *Powder Diffr.* **21**, 67 (2006).
- [34] F. Amann, R. Poulain, S. Delannoy, R. Guillou, M. Talla Noutack, Z. Kloenne, S. Nowak, J.-P. Couzinié, F. De Geuser, D. Thiaudière, J.-L. Béchade, E. Clouet, H. Fraser, I. Guillot, and F. Prima, On the oxygen ordering mechanisms in dilute Ti-Zr-O systems, in *15th World Conference on Titanium* (to be published).
- [35] Z. Liu and G. Welsch, Literature survey on diffusivities of oxygen, aluminum, and vanadium in alpha titanium, beta titanium, and in rutile, *Metall. Trans. A* **19**, 1121 (1988).
- [36] Y. S. Touloukian, R. K. Kirby, R. Taylor, and P. D. Desai, *Thermal Expansion - Metallic Elements and Alloys*, Thermophysical Properties of Matter Thermal Expansion Vol. 12 (Plenum, New York, 1975).
- [37] P. Souvatzis, O. Eriksson, and M. I. Katsnelson, Anomalous thermal expansion in α -titanium, *Phys. Rev. Lett.* **99**, 015901 (2007).
- [38] Z.-G. Mei, S.-L. Shang, Y. Wang, and Z.-K. Liu, Density-functional study of the thermodynamic properties and the pressure-temperature phase diagram of Ti, *Phys. Rev. B* **80**, 104116 (2009).
- [39] J. P. Perdew and A. Zunger, Self-interaction correction to density-functional approximations for many-electron systems, *Phys. Rev. B* **23**, 5048 (1981).